Novel Varactor-Tuned Coupling Mechanism and Its Applications to High-Order Bandwidth-Agile Bandpass Filters

Jing Cai, *Member, IEEE*, Wei Qin, Jian-Xin Chen, *Member, IEEE*, and Quan Xue, *Fellow, IEEE*

***Abstract*— In this paper, a novel tunable coupling mechanism with bandwidth-tunable capability is presented. Metallic via has been utilized to construct the coupling structure, namely via-coupling. Studies show that the via-coupling mechanism provides more flexibility and owns better tolerance to fabrication errors than the traditional gap-coupling. By employing varactor in parallel with the metallic via, the coupling coefficient between each resonator pairs can be effectively tuned. It is worth noting that only one varactor is required for each resonator pair. The lumped-circuit model of the tunable coupling mechanism is investigated and extracted by classical theory derivation and simple programming. For verification, a fourth-order quasi-elliptic bandpass filter (BPF) and a bandwidth-tunable one are designed, fabricated, and measured. For the bandwidth-tunable BPF, the factional bandwidth varies from 2.52% to 5.04%, meaning a double tuning range. The in-band insertion loss varies from 2.8 to 4.8 dB, and the return loss is better than 17 dB. If needed, BPFs with Nth-order ($N > 4$) could be designed based on the proposed tunable coupling mechanism and only ($N + 1$) varactors are required.**

***Index Terms*— Bandpass filter (BPF), bandwidth tunable, gap-coupling, quasi-elliptic response, varactor, via-coupling.**

I. Introduction

RECENTLY, microwave systems with multiband and multifunction become more and more attractive due to the increasing demand of modern wireless communications. Such systems mainly require circuits and components owning capabilities of dealing with different frequency bands and/or bandwidths. Accordingly, tunable microwave filter, which is an essential component for reconfigurable front ends, emerges as a very hot topic in microwave area. Various kinds of tunable filters have been developed by using semiconductor varactors, microelectromechanical system technology [1]–[3], yttrium–iron–garnet technology [4], piezoelectric transducers [5], and so on. Among them, varactor-tuned bandpass filters (BPFs) are widely researched and explored due to their small size, rapid tuning speed, and low cost [6]–[24].

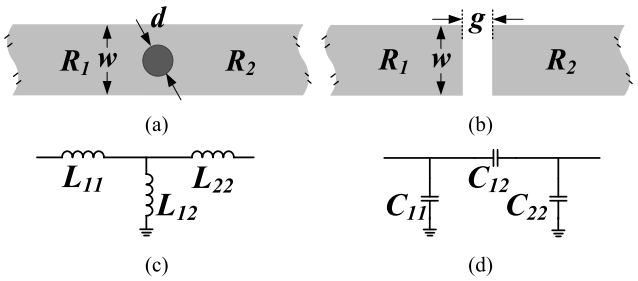

Fig. 1. (a) Diagram of the via-coupling. (b) Diagram of the gap-coupling. (c) Lumped-circuit model for the via structure. (d) Lumped-circuit model for the gap structure.

In the past decades, research on tunable BPFs mainly focuses on controlling center frequency of the passband [6]–[16]. Recently, a few works develop BPFs with bandwidth tunability [17]–[24]. Among them, two famous methods have been applied to realize bandwidth control. One method is to control couplings between resonators [17]–[20]. In [17], for example, a varactor pair is symmetrically added between each resonator pair so as to control the coupling level. However, the employment of numerous varactors will enlarge total insertion loss and fabrication cost, especially for the higher order bandwidth-tunable BPFs. The other method is to control different frequency modes of multimode resonator by disposing varactor diodes at the specific positions of the resonator [21], [22]. For instance, a tunable wideband BPF based on a stub-loaded triple-mode resonator is presented in [22], and bandwidth tunability is realized by tuning different frequency modes. However, this method cannot be easily utilized in higher order bandwidth-tunable BPFs. Therefore, further research on higher order BPFs with bandwidth tunability by using as few as varactors needs to be conducted.

In this paper, a novel tunable coupling mechanism, which is realized by one ordinary metallic via and one varactor to tune the coupling level between each resonator pair, is investigated. First, the coupling mechanism using metallic via, namely via-coupling [see Fig. 1(a)], is carefully studied and

Manuscript received October 6, 2016; revised December 28, 2016; accepted December 31, 2016. This work was supported in part by the National Natural Science Foundation of China under Grant 61501263 and Grant 61271136, in part by the Graduate Research and Innovation Plan Project of the Universities of Jiangsu Province under Grant KYLX16_0971, and in part by the Nantong University-Nantong Joint Research Center for Intelligent Information Technology. Recommended for publication by Associate Editor T.-L. Wu upon evaluation of reviewers' comments.

J. Cai, W. Qin, and J.-X. Chen are with the School of Electronics and Information, Nantong University, Nantong 226019, China, and also with Nantong Research Institute for Advanced Communication Technologies, Nantong 226019, China (e-mail: waiky.w.qin@hotmail.com).

Q. Xue is with the State Key Laboratory of Millimeter Waves, Department of Electronic Engineering, City University of Hong Kong, Hong Kong, and also with City University of Hong Kong Shenzhen Research Institute, City University of Hong Kong, Hong Kong.

Color versions of one or more of the figures in this paper are available online at http://ieeexplore.ieee.org.

Digital Object Identifier 10.1109/TCPMT.2017.2647745

compared to the traditional gap-coupling [see Fig. 1(b)] in end-coupled structure. The comparison shows that the via-coupling features better fabrication tolerance and more design flexibility, which is significant in industrial applications. Then, the working principle of the proposed tunable via-coupling is presented. Based on this tuning structure, a fourth-order quasi-elliptic BPF with bandwidth control is designed, fabricated, and measured as an example for verification. Because only one varactor is needed between each resonator pair, the proposed bandwidth-tunable BPF requires fewer varactors as compared to previous relevant works. Moreover, the proposed BPF possesses the via-couplings as main couplings and the gap-coupling as cross-coupling, resulting in high selectivity for the passband.

II. Tunable Via-Coupling Mechanism

In modern microwave devices and systems, metallic vias are generally employed as shorting pins to connect metals at different layers. As the development of the PCB process, metallic vias can be easily and accurately manufactured by chemical electroplating technique or silver conductive paste baking technique. Both the diameter and position of a metallic via can be precisely defined in the fabrication process. In this section, the characteristics of the via-coupling are studied by means of both the coupling coefficient and the lumped-circuit model.

A. Comparison Between Via-Coupling and Gap-Coupling

The via-coupling can be realized by sharing one metallic via between two short-ended resonators as shown in Fig. 1(a). Similarly, as shown in Fig. 1(b), the diagram of the traditional gap-coupling is achieved by the gaps between two open-ended resonators. For the sake of comparing and analyzing, the via-coupling and gap-coupling are investigated under the identical conditions. In this section, the coupling coefficient is used for analysis.

According to the coupled resonator theory, the coupling coefficient between two coupled resonators with the same resonant frequencies can be extracted by the following equation:

$$M = \pm \left| \frac{f_{p2}^2 - f_{p1}^2}{f_{p2}^2 + f_{p1}^2} \right| \tag{1}$$

where f_{p1} and f_{p2} denote the two split resonant frequencies of the coupling structure.

By using (1), the coupling coefficients of the via-coupling versus normalized line widths w/h and normalized via diameters d/h are shown as the curves in Fig. 2(a), where h is the height of the substrate. Similarly, Fig. 2(b) shows the absolute values of the gap-couplings versus normalized widths w/h and normalized gaps g/h. By comparing Fig. 2(a) and (b), it can be seen that the via-coupling decreases moderately and smoothly as d/h increases (not too sensitive to the physical parameters), while the gap-coupling decreases rapidly in the strong coupling region (especially when g/h is below 0.3). It means that in the strong coupling region, the fabrication tolerance of the via-coupling is much better than that of the gap-coupling. It is also fortunate to find that

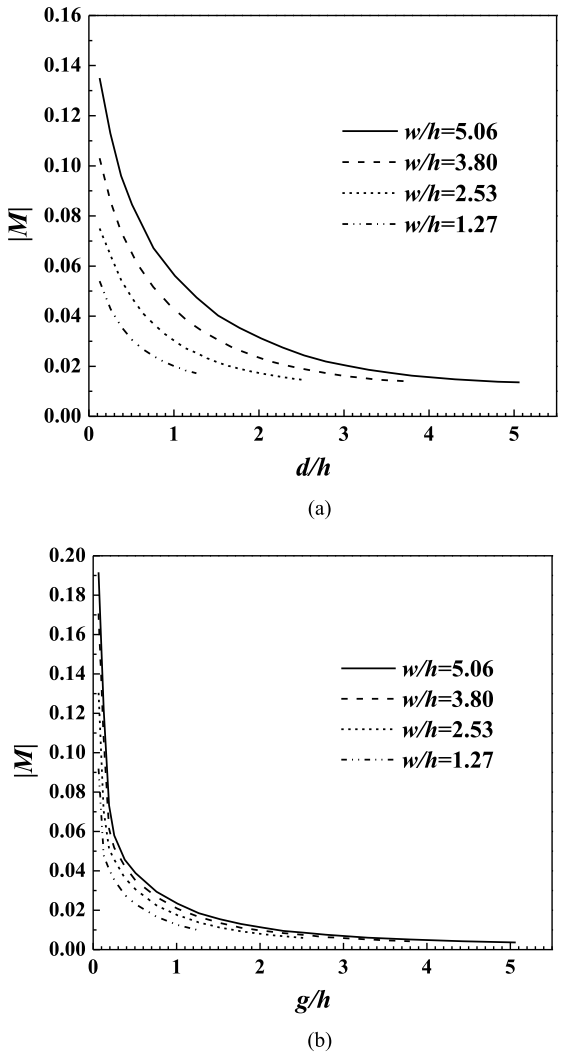

Fig. 2. Coupling coefficients $|M|$ versus normalized widths w/h or normalized diameters d/h. (a) Via-coupling. (b) Gap-coupling.

the gap-coupling also changes smoothly in the weak coupling region (g/h is over 0.5). It means that the gap-coupling also owns good fabrication tolerance in such region. In BPF designs, the cross-couplings, which are generally weaker than the main couplings, can be applied to improve the sideband selectivity. Therefore, it is considered that a BPF with the via-couplings as the main couplings and the gap-couplings as the cross-couplings would own high selectivity and excellent fabrication tolerance simultaneously. Based on this concept, a quasi-elliptic response BPF will be designed in Section III-A.

B. Determination of Lumped-Circuit Model of Via-Coupling

In addition to the coupling coefficient, the lumped-circuit model will also be helpful in understanding the characteristics of the coupling mechanism. Ignoring radiation and material losses, the lumped-circuit models of the via structure and gap structure are shown in Fig. 1(c) and (d), respectively. The series inductors, L_{11} and L_{22}, are to model the current changes, which caused by the metallic via (usually $L_{11} = L_{22}$); the parallel L_{12} models the inductance

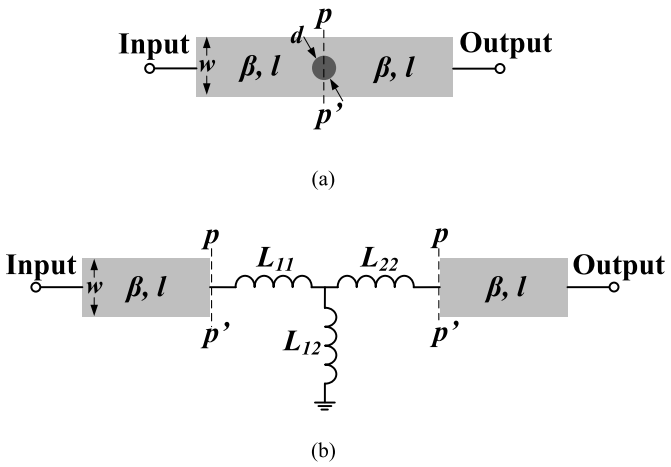

Fig. 3. (a) Diagram of the simplest via-coupling where imaginary line p-p' is the central division line. (b) Circuit model of the via-coupling in which the metallic via is replaced by its lump-element circuit model.

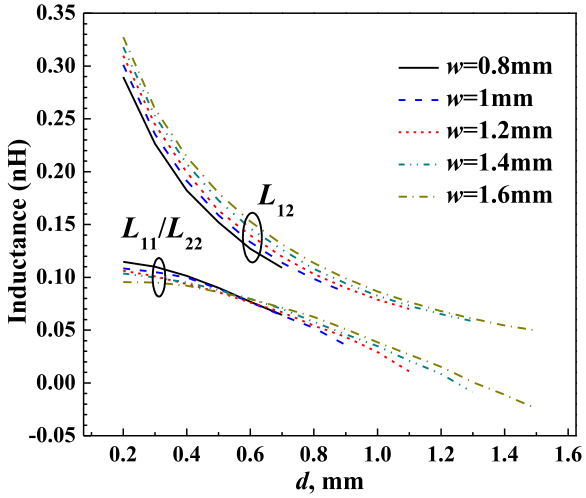

Fig. 4. Calculated values of L_{11}/L_{22} and L_{12}.

of the metallic via itself. Similarly, the parallel capacitors, C_{11} and C_{22}, represent the end capacitances to the ground; series C_{12} is the gap capacitance between the two resonators.

To contribute to the study of coupling tunability, a method to extract the lumped parameters (L_{11}/L_{22} and L_{12}) of the via-coupling structure is presented. As shown in Fig. 3(a), the metallic via is set at the middle (reference plane p-p') of the transmission line to form a two-port network, where β and l are the propagation constant and the physical length of the transmission line, respectively. Then, this network is simulated in Ansoft HFSS to obtain its S-parameters, denoted as $[S_N]$. The equivalent circuit model of Fig. 3(a) is given in Fig. 3(b), where the metallic via is replaced by its lumped-circuit model. Accordingly, the *ABCD* matrix $[A]$ of the model in Fig. 3(b) can be obtained as follows:

$$[A] = [A_1][A_2][A_3][A_2][A_1] \tag{2}$$

where

$$[A_1] = \begin{bmatrix} \cos\beta l & jZ_0 \sin\beta l \\ jY_0 \sin\beta l & \cos\beta l \end{bmatrix} \tag{3a}$$

$$[A_2] = \begin{bmatrix} 1 & j\omega L_{11} \\ 0 & 1 \end{bmatrix} \tag{3b}$$

$$[A_3] = \begin{bmatrix} 1 & 0 \\ \dfrac{1}{j\omega L_{12}} & 1 \end{bmatrix}. \tag{3c}$$

As mentioned above, $[A_1]$, $[A_2]$, and $[A_3]$ are the *ABCD* matrix of the transmission line, L_{11}/L_{22} and L_{12}, respectively. Z_0 and Y_0 are the characteristic impedance and admittance of the transmission line. By transforming $[A]$ into the scattering parameters matrix $[S_E]$ and making $[S_E] = [S_N]$, the values of L_{11}/L_{22} and L_{12} can be calculated by means of simple programing. Accordingly, the relationship between the equivalent inductances and the physical parameters is extracted and shown in Fig. 4, where the substrate used is the Rogers *RO4003C* with a relative permittivity of 3.38 and a thickness of 0.813 mm. The extraction of the equivalent inductances will be very helpful and instructive for constructing the tunable via-coupling structure in Section II-C.

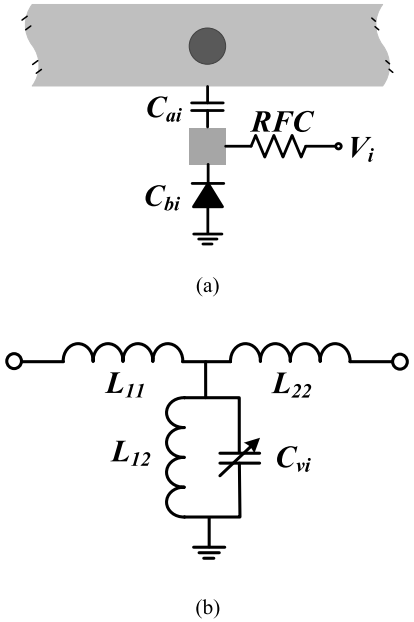

Fig. 5. (a) Diagram of the tunable via-coupling structure where RFC means the RF choke realized by a resistor with a large value of 50 KΩ. (b) Lumped-circuit model for the tunable via-coupling structure.

C. Novel Tunable Via-Coupling Mechanism

According to the investigation of the lumped-circuit model for the via-coupling, it is found that the via-coupling possesses a potential capability of tunability. As shown in Fig. 5(a), an electronic tuning circuit is attached to the resonator, in which $C_{\rm ai}$ is the capacitor for dc block, C_{bi} is the varactor for tuning, and RFC represents a resistor with a large value of 50 KΩ for RF choke. This tuning circuit is set at the geometric center and in parallel with the metallic via. Accordingly, the equivalent model of tunable via-coupling can be presented as shown in Fig. 5(b), where the tunable capacitance C_{vi} can be

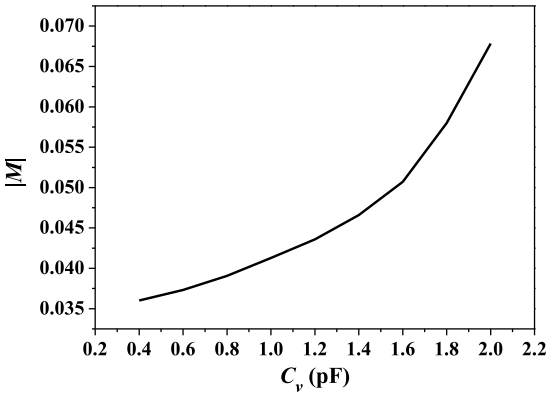

Fig. 6. Simulated result of coupling coefficient versus the capacitance of C_v. (under the situation of L_{11} or $L_{22} = 0.05$ nH and $L_{12} = 0.1$ nH).

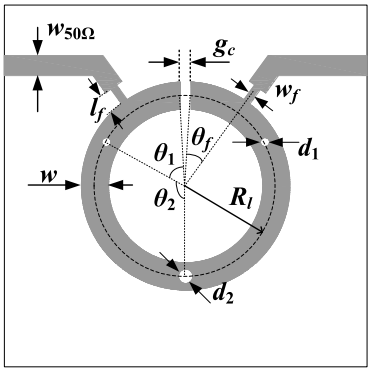

Fig. 7. Layout of the proposed end-coupled BPF with quasi-elliptic response.

obtained as

$$C_{vi} = \frac{C_{ai}C_{bi}}{C_{ai} + C_{bi}}, \quad i = 1, 2, 3 \ldots. \tag{4}$$

Due to the utilization of C_{vi}, the coupling coefficient of the via-coupling can be effectively tuned. Fig. 6 shows the changing of C_v against coupling coefficient when L_{11} or $L_{22} = 0.05$ nH, and $L_{12} = 0.1$ nH for $w = 1.2$ mm and $d = 0.8$ mm. As can be seen, the coupling coefficient increases with the value of C_v, resulting that the bandwidth will be broadened. This novel bandwidth-tunable mechanism only needs one varactor between each two resonators, which means the parasitic effect of varactor can be reduced. It is especially important for the higher order BPF designs.

III. Filter Designs

To verify the applicability of the via-coupling, a fourth-order quasi-elliptic response BPF is designed. Based on it, a four-order BPF with bandwidth agility is also designed to show the advantage of the novel tuning structure.

A. Fourth-Order Quasi-Elliptic Response BPF

In most wireless communication systems, BPFs with high selectivity are more desirable. A most popular method to realize high-selectivity BPFs without enlarging the circuit size is to generating transmission zeros (TZs) close to the passbands by introducing cross-couplings between nonadjacent resonators. For a fourth-order BPF with cross-coupling between the first and fourth resonators, two TZs can be easily generated to obtain a quasi-elliptic frequency response. The condition is that the cross-coupling should have an opposite sign to the main couplings so that signals from the two paths will eliminate each other at certain frequencies. It is the signal elimination that generates TZs. Based on this concept, a fourth-order end-coupled BPF with quasi-elliptic response is proposed by combining the via- and gap-couplings. Its layout is shown in Fig. 7. The first and fourth resonators are $\lambda/4$ resonators, while the second and third resonators are $\lambda/2$. All the resonators are bended to form a split ring so that the open ends of the two $\lambda/4$ uniform impedance resonators (UIRs) can couple to each other through the gap-coupling. The gap-coupling contributes to the cross-coupling, which has an opposite sign to the main via-couplings. The physical lengths of the $\lambda/4$ and $\lambda/2$ resonators are approximately equal to $R_l\theta_1$ and $R_l\theta_2$, respectively. The main via-couplings depend on the diameters d_1 and d_2, while the cross-coupling is controlled by the coupling gap g_c. The feeding point is dependent on $R_l\theta_f$.

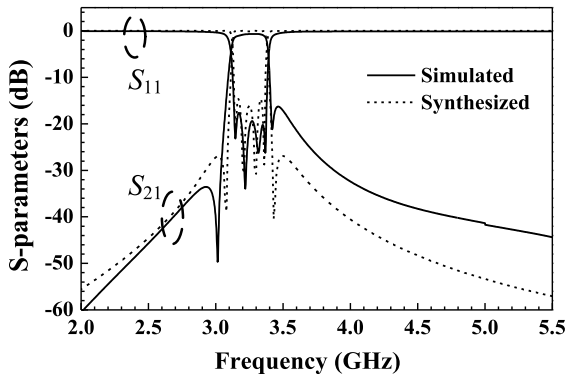

Fig. 8. Synthesized and simulated results for the designed quasi-elliptic response BPF.

If a quasi-elliptic BPF with a center frequency of 3.25 GHz, a 0.2-dB-ripple fractional bandwidth (*FBW*) of 7.4%, and two TZs at 3.1/3.4 GHz are required, the coupling matrix and the external quality factor Q_E can be generated as follows [25]:

$$[M] = \begin{bmatrix} 0 & 0.052 & 0 & -0.015 \\ 0.052 & 0 & 0.052 & 0 \\ 0 & 0.052 & 0 & 0.052 \\ -0.015 & 0 & 0.052 & 0 \end{bmatrix}$$
$$Q_E = 17.5. \tag{5}$$

Accordingly, the physical parameters can be obtained: $w_{50\Omega} = 2.2$ mm, $w_f = 0.4$ mm, $l_f = 2.0$ mm, $\theta_f = 49.2°$, $w = 3$ mm,$R_l = 15.0$ mm, $\theta_1 = 58.7°$, $\theta_2 = 119.0°$, $d_1 = 0.6$ mm, $d_2 = 0.6$ mm, and $g_c = 1.2$ mm. Fig. 8 shows the simulated responses of the designed quasi-elliptic BPF together with the synthesized results for comparison. Good agreements have been observed except the slight shifts in the TZs. The shifts are because of a small quantity of power leaking from the first/second resonators to the third/fourth resonators, resulting a nonzero M_{13} and M_{24} in the coupling matrix. There is one important thing to mention that the

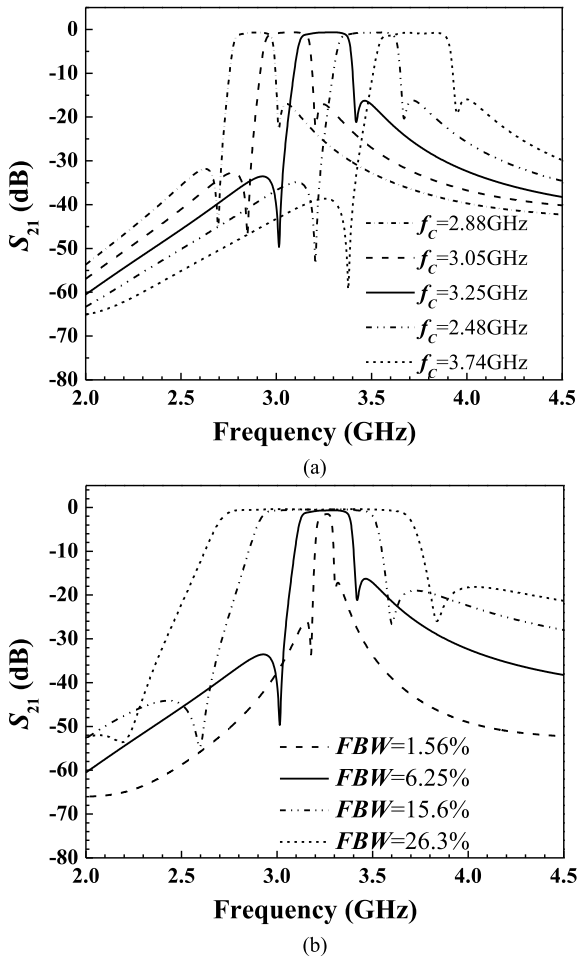

Fig. 9. Simulated S_{21} of quasi-elliptic response BPFs with different (a) center frequencies and (b) fractional bandwidths.

cross-coupling gap (g_c) is in the weak coupling region of Fig. 2(b). Therefore, all the coupling parameters (g_c, d_1, and d_2) are insensitive to fabrication errors. This means the proposed structure still owns excellent fabrication tolerance although the gap-coupling is used.

This proposed design has high flexibility of tuning not only for its center frequency, but also for its bandwidth. By just changing the radius of the ring, R_l, the center frequency of the passband can be tuned without affecting the *FBW*, which is shown in Fig. 9(a). Fig. 9(b) shows the transmission responses (S_{21}) of BPFs with the same center frequencies and different *FBWs*. The *FBW* varies in a wide dynamic range, from 1.56% to 26.3%. To obtain Fig. 9(b), we change w and keep d_1 and d_2 unchanged first so that the *FBW* varies. However, the center frequency will be also affected by w. Then, according to Fig. 9(a), the center frequency could be fine tuning to remain the same by changing R_l. In a conclusion, the proposed structure shows much flexibility in quasi-elliptic response BPF design, giving a theoretical basis for electrically tuning.

B. Fourth-Order Bandwidth-Tunable BPF

Fig. 10 shows the layout of the proposed bandwidth-tunable BPF. In this section, the physical parameters are determined

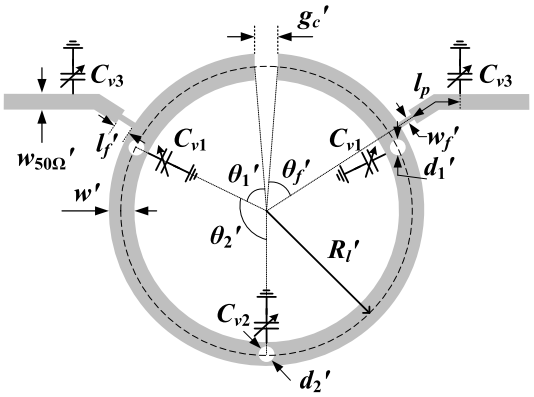

Fig. 10. Layout of the proposed bandwidth-tunable BPF.

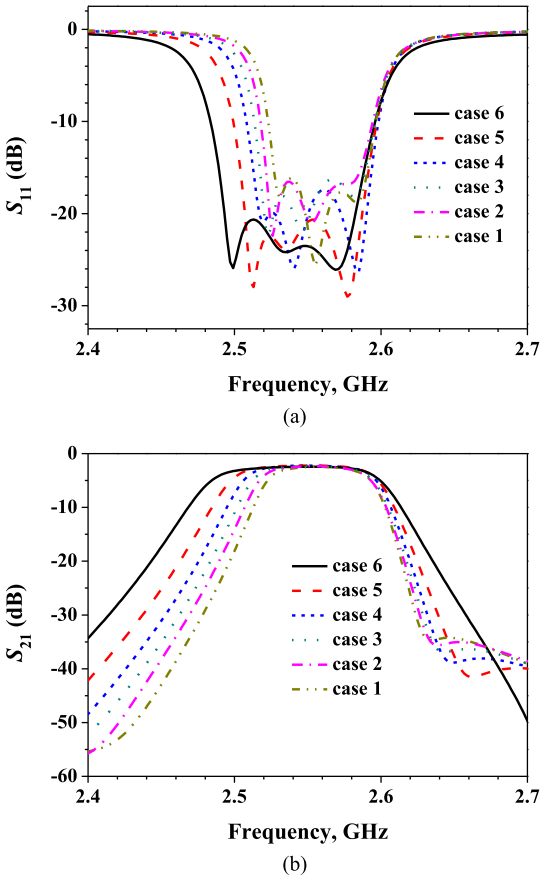

Fig. 11. Simulated results of the bandwidth-tunable BPF. (a) S_{11}. (b) S_{21}.

to form a good passband performance after optimization: $w'_{50\Omega} = 1.8$ mm, $w'_f = 0.4$ mm, $l'_f = 2.0$ mm, $\theta'_f = 52.8°$, $w' = 1.2$ mm, $R'_l = 17.3$ mm, $\theta'_1 = 57.8°$, $\theta'_2 = 117.6°$, $d'_1 = 0.8$ mm, $d'_2 = 0.8$ mm, and $g'_c = 2.6$ mm. The substrate used is the Rogers *RO4003C* with a relative permittivity of 3.38 and a thickness of 0.813 mm. To realize bandwidth tuning and maintain good passband performance, five varactors are added to tune the couplings and Q_E. Among them, three varactors are attached in parallel with the metallic via to realize the tunable coupling coefficient and the other two are set at the feeding line to make Q_E keeping appropriate when the

TABLE I
DETAILED SIMULATION VALUES OF VARACTORS

Cases	1	2	3	4	5	6
C_{b1} (pF)	0.57	0.93	1.6	2.6	3.7	4.8
C_{b2} (pF)	0.63	1.7	2.6	3.6	4.2	5.2
C_{b3} (pF)	0.5	0.7	1.7	5.5	7.3	8.5

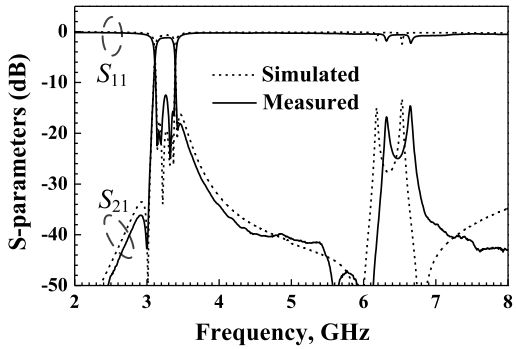

Fig. 12. Measured and simulated results for the fabricated quasi-elliptic response BPF.

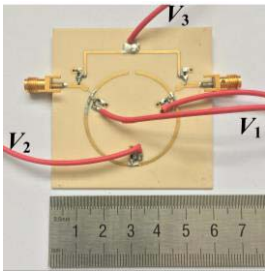

Fig. 13. Photograph of the fabricated fourth-order bandwidth-tunable BPF.

coupling coefficient is tuned. The varactor diodes JDV2S71E from Toshiba with a tunable capacitance of 0.57–9 pF are used and the dc blocks C_{a1}, C_{a2}, and C_{a3} are chosen as 2.5, 2.5, and 0.5 pF, respectively. Fig. 11 shows the simulated responses of the designed bandwidth-tunable BPF, where the corresponding values of C_{vi} for six different cases are listed in Table I. It can be observed that the center frequency of the passband will be shifted during the bandwidth tuning. The reason is that the coupling tuning between two coupled resonators is actually realized by tuning one of the split resonant frequency with the other being almost unchanged. It should be mentioned that $(N + 1)$ varactors are required for an Nth-order bandwidth-tunable BPF.

IV. MEASUREMENT

For the purpose of verification, the above-mentioned BPFs are fabricated and measured by Agilent E8363C network analyzer.

A. Fourth-Order Quasi-Elliptic Response BPF

The BPF designed in Section III-A is fabricated and measured. Its measured and simulated results are shown in Fig. 12. Good agreements are observed, implying tolerance to fabrication errors to a certain extent. The measured in-band insertion loss, including the loss from SMA connectors, is around 1.2 dB and the in-band return loss is greater than 12 dB. Two TZs are realized close to the passband edge at 3 and 3.42 GHz, which guarantee high selectivity. The second-order harmonic is suppressed to some extend because two $\lambda/4$ UIRs are employed.

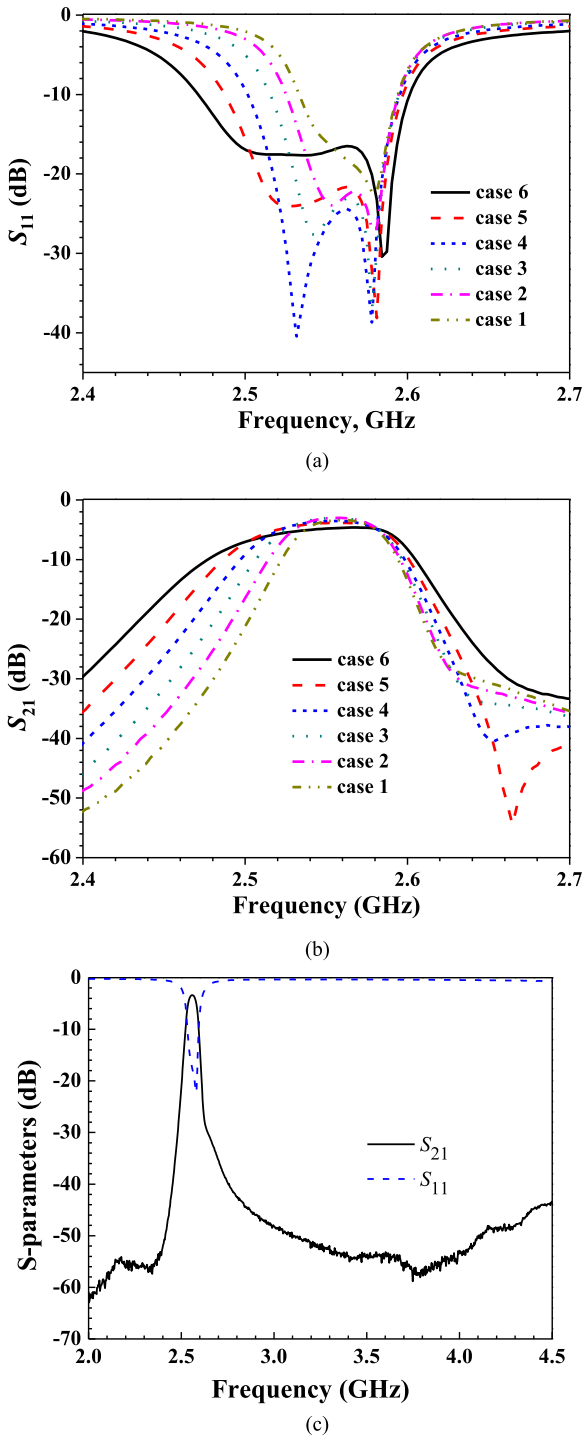

Fig. 14. Measured results of the bandwidth-tunable BPF. (a) Narrowband view of S_{11}. (b) Narrowband view of S_{21}. (c) Broadband view of case 1.

B. Fourth-Order Bandwidth-Tunable BPF

The bandwidth-tunable BPF mentioned previously has also been fabricated measured to verify the characteristics of the

TABLE II
DETAILED VALUES OF BIAS VOLTAGES

Cases	1	2	3	4	5	6
V_1 (V)	30	12	7.5	4.5	3	2
V_2 (V)	20	7	4.5	3.15	2.5	1.75
V_3 (V)	30	17	7	1.6	0.7	0

TABLE III
COMPARISON TO PREVIOUS BANDWIDTH-TUNABLE BPFS

	Filter order/ varactor number	*FBW* tuning range (%)	Insertion loss(dB)	Return loss (dB)	Size($\lambda_g \times \lambda_g$)
[17]	4/10	2.2-8	5.2-6.2	N/A	0.2×0.28
[18]	2/9	2.2-11.2	3.1-15.6	N/A	0.18×0.25
[21]	4/6	22-34	0.8	11	N/A
[22]	3/6	14-64.4	1-2	15	N/A
[23]	2/6	5.76-8.55	1.99-4.42	9	0.16×0.23
		8.28-12.42	1.64-4.2	9	
[24]	2/6	4-12	1-3	9	0.11×0.11
This work	4/5	2.52-5.04	3-4.76	17	0.16×0.14

proposed tunable coupling mechanism. Fig. 13 shows its photograph. The simulated and measured results are shown in Fig. 14. The detailed values of bias voltages V_i ($i = 1, 2, 3$) for six different cases have been given in Table II. The in-band insertion loss, including the loss from SMA connectors and the varactor-diodes, varies from 2.8 to 4.8 dB. The measured return loss is better than 17 dB. The *FBW* changes from 2.52% to 5.04%, which means a double tuning range. It can be seen from Fig. 14(c) that the proposed bandwidth-tunable BPF does also feature good stopband rejection performance.

Table III summarizes the comparison of the proposed design to the previous bandwidth-tunable BPFs. As can be seen, the proposed filter features competitive performance, such as number of varactors, insertion loss, and return loss, making it a good candidate for higher order bandwidth-tunable BPFs.

V. CONCLUSION

In this paper, a novel tunable coupling mechanism is investigated and the corresponding bandwidth-tunable BPF is presented. The proposed via-coupling features better fabrication tolerance as compared to the traditional gap-coupling, which is useful and attractive in many practical and industrial applications. The insertion loss of the designed bandwidth-tunable BPF is comparatively small because only one varactor-diode is required for each coupling. Moreover, higher order designs can be conveniently realized, showcasing a promising choice for modern and future communication systems.

REFERENCES

[1] Y. Shim, Z. Wu, and M. Rais-Zadeh, "A high-performance continuously tunable MEMS bandpass filter at 1 GHz," *IEEE Trans. Microw. Theory Techn.*, vol. 60, no. 8, pp. 2439–2447, Aug. 2012.

[2] M. Nosrati, N. Vahabisani, and M. Daneshmand, "Compact MEMS-based ultrawide-band CPW band-pass filters with single/double tunable notch-bands," *IEEE Trans. Compon., Packag., Manuf. Technol.*, vol. 4, no. 9, pp. 1451–1460, Sep. 2014.

[3] L. Pelliccia, F. Cacciamani, P. Farinelli, and R. Sorrentino, "High-Q tunable waveguide filters using ohmic RF MEMS switches," *IEEE Trans. Microw. Theory Techn.*, vol. 63, no. 10, pp. 3381–3390, Oct. 2015.

[4] Y. Murakami, T. Ohgihara, and T. Okamoto, "A 0.5–4.0-GHz tunable bandpass filter using YIG film grown by LPE," *IEEE Trans. Microw. Theory Techn.*, vol. MTT-35, no. 12, pp. 1192–1198, Dec. 1987.

[5] M. S. Tong and C. X. Yang, "VSIE-based scattering parameter analysis for a tunable bandpass filter with a PET-controlled magnetodielectric perturber," *IEEE Trans. Compon., Packag., Manuf. Technol.*, vol. 5, no. 5, pp. 661–667, May 2015.

[6] H.-Y. Tsai, T.-Y. Huang, and R.-B. Wu, "Varactor-tuned compact dual-mode tunable filter with constant passband characteristics," *IEEE Trans. Compon., Packag., Manuf. Technol.*, vol. 6, no. 9, pp. 1399–1407, Sep. 2016.

[7] X. Y. Zhang, Q. Xue, C. H. Chan, and B.-J. Hu, "Low-loss frequency-agile bandpass filters with controllable bandwidth and suppressed second harmonic," *IEEE Trans. Microw. Theory Techn.*, vol. 58, no. 6, pp. 1557–1564, Jun. 2010.

[8] X.-G. Wang, Y.-H. Cho, and S.-W. Yun, "A tunable combline bandpass filter loaded with series resonator," *IEEE Trans. Microw. Theory Techn.*, vol. 60, no. 6, pp. 1569–1576, Jun. 2012.

[9] G. Chaudhary, Y. Jeong, and J. Lim, "Harmonic suppressed dual-band bandpass filters with tunable passbands," *IEEE Trans. Microw. Theory Techn.*, vol. 60, no. 7, pp. 2115–2123, Jul. 2012.

[10] C. Li *et al.*, "A tunable high temperature superconducting bandpass filter realized using semiconductor varactors," *IEEE Trans. Appl. Supercond.*, vol. 24, no. 5, pp. 1–5, Oct. 2014.

[11] B. You, L. Chen, Y. Liang, and X. Wen, "A high-selectivity tunable dual-band bandpass filter using stub-loaded stepped-impedance resonators," *IEEE Microw. Wireless Compon. Lett.*, vol. 24, no. 11, pp. 736–738, Nov. 2014.

[12] Q. Xiang, Q. Feng, X. Huang, and D. Jia, "Electrical tunable microstrip LC bandpass filters with constant bandwidth," *IEEE Trans. Microw. Theory Techn.*, vol. 61, no. 3, pp. 1124–1130, Mar. 2013.

[13] M. A. El-Tanani and G. M. Rebeiz, "Corrugated microstrip coupled lines for constant absolute bandwidth tunable filters," *IEEE Trans. Microw. Theory Techn.*, vol. 58, no. 4, pp. 956–963, Apr. 2010.

[14] C.-W. Tang, C.-T. Tseng, and S.-C. Chang, "Design of the compact tunable filter with modified coupled lines," *IEEE Trans. Compon., Packag., Manuf. Technol.*, vol. 4, no. 11, pp. 1815–1821, Nov. 2014.

[15] J.-X. Chen, Y. Ma, J. Cai, L.-H. Zhou, Z.-H. Bao, and W. Che, "Novel frequency-agile bandpass filter with wide tuning range and spurious suppression," *IEEE Trans. Ind. Electron.*, vol. 62, no. 10, pp. 6428–6435, Oct. 2015.

[16] X. Huang, L. Zhu, Q. Feng, Q. Xiang, and D. Jia, "Tunable bandpass filter with independently controllable dual passbands," *IEEE Trans. Microw. Theory Techn.*, vol. 61, no. 9, pp. 3200–3208, Sep. 2013.

[17] Y.-C. Chiou and G. M. Rebeiz, "Tunable 1.55–2.1 GHz 4-pole elliptic bandpass filter with bandwidth control and >50 dB rejection for wireless systems," *IEEE Trans. Microw. Theory Techn.*, vol. 61, no. 1, pp. 117–124, Jan. 2013.

[18] Y.-C. Chiou and G. M. Rebeiz, "A tunable three-pole 1.5–2.2-GHz bandpass filter with bandwidths and transmission zero control," *IEEE Trans. Microw. Theory Techn.*, vol. 59, no. 11, pp. 2872–2878, Nov. 2011.

[19] Y.-H. Cho and G. M. Rebeiz, "0.7–1.0-GHz reconfigurable bandpass-to-bandstop filter with selectable 2- and 4-pole responses," *IEEE Trans. Microw. Theory Techn.*, vol. 62, no. 11, pp. 2626–2632, Nov. 2014.

[20] Y.-C. Chiou and G. M. Rebeiz, "A quasi elliptic function 1.75–2.25 GHz 3-pole bandpass filter with bandwidth control," *IEEE Trans. Microw. Theory Techn.*, vol. 60, no. 2, pp. 244–249, Feb. 2012.

[21] X. Huang, Q. Feng, and Q. Xiang, "Bandpass filter with tunable bandwidth using quadruple-mode stub-loaded resonator," *IEEE Microw. Wireless Compon. Lett.*, vol. 22, no. 4, pp. 176–178, Apr. 2012.

[22] J.-R. Mao, W.-W. Choi, K.-W. Tam, W. Q. Che, and Q. Xue, "Tunable bandpass filter design based on external quality factor tuning and multiple mode resonators for wideband applications," *IEEE Trans. Microw. Theory Techn.*, vol. 61, no. 7, pp. 2574–2584, Jul. 2013.

[23] G. Chaudhary, Y. Jeong, and J. Lim, "Dual-band bandpass filter with independently tunable center frequencies and bandwidths," *IEEE Trans. Microw. Theory Techn.*, vol. 61, no. 1, pp. 107–116, Jan. 2013.

[24] A. L. C. Serrano, F. S. Correra, T.-P. Vuong, and P. Ferrari, "Synthesis methodology applied to a tunable patch filter with independent frequency and bandwidth control," *IEEE Trans. Microw. Theory Techn.*, vol. 60, no. 3, pp. 484–493, Mar. 2012.

[25] J.-S. Hong and M. J. Lancaster, *Microstrip Filters for RF/Microwave Applications*. New York, NY, USA: Wiley, 2004.

Jing Cai was born in Nantong, China, in 1992. He received the B.Sc. degree from Nantong University, Nantong, in 2015, where he is currently pursuing the M.Sc. degree in electromagnetic field and microwave technology.

His current research interests include tunable and reconfigurable microwave circuits.

Wei Qin (S'09–M'14) was born in Jiangsu, China. He received the B.Sc. degree in electronic engineering and the M.Sc. degree in electromagnetic fields and microwave technology from Southeast University, Nanjing, China, in 2007 and 2010, respectively, and the Ph.D. degree in electronic engineering from the City University of Hong Kong, Hong Kong, in 2013.

In 2013, he joined the State Key Laboratory of Millimeter Waves, City University of Hong Kong, as a Senior Research Associate. Since 2014, he has been with the School of Electronics and Information, Nantong University, Nantong, China, where he is currently an Associate Professor. His current research interests include the design and application of microwave devices and antennas.

Jian-Xin Chen (M'08) was born in Nantong, China, in 1979. He received the B.S. degree from the Huaiyin Teachers College, Huai'an, China, in 2001, the M.S. degree from the University of Electronic Science and Technology of China, Chengdu, China, in 2004, and the Ph.D. degree from the City University of Hong Kong, Hong Kong, in 2008.

Since 2009, he has been with Nantong University, Nantong, where he is currently a Professor. He has authored or coauthored over 80 internationally referred journal and conference papers. He holds five Chinese patents and two U.S. patents. His current research interests include microwave active/passive circuits and antennas and LTCC-based millimeter-wave circuits and antennas.

Dr. Chen was a recipient of the Best Paper Award presented at the Chinese National Microwave and Millimeter-Wave Symposium, Ningbo, China, in 2007. He was the Supervisor of 2014 iWEM student innovation competition winner in Sapporo, Japan.

Quan Xue (M'02–SM'04–F'11) received the B.S., M.S., and Ph.D. degrees in electronic engineering from the University of Electronic Science and Technology of China (UESTC), Chengdu, China, in 1988, 1990, and 1993, respectively.

In 1993, he joined UESTC as a Lecturer, then became a Professor in 1997. From 1997 to 1998, he was a Research Associate and then a Research Fellow with The Chinese University of Hong Kong, Hong Kong. In 1999, he joined the City University of Hong Kong (CityU), Hong Kong, where he is currently a Chair Professor of microwave engineering and also serves as the Director of the Information and Communication Technology Center, the Deputy Director of CityU Shenzhen Research Institute, and the Deputy Director of the State Key Laboratory of Millimeter Waves. He has authored or coauthored over 260 internationally referred journal papers and over 100 international conference papers. His current research interests include microwave passive components, active components, antenna, microwave monolithic integrated circuits, and radio-frequency integrated circuits.

Dr. Xue served as the IEEE AdCom Member of MTT-S from 2011 to 2013, and an Associate Editor of the IEEE TRANSACTIONS ON MICROWAVE THEORY AND TECHNIQUES from 2010 to 2013. He has been an Associate Editor of the IEEE TRANSACTIONS ON INDUSTRIAL ELECTRONICS since 2010. He was the Associate Vice-President with Innovation Advancement and China Office from 2011 to 2015.